

Article

Residual Shear Capacity of RC Beams without Stirrups after Fire Exposure

Yamin Song^{1,2,*}, Chuanguo Fu³ and Shuting Liang²¹ School of Civil Engineering, Don College of Shandong Jiaotong University, Jinan 250357, China² School of Civil Engineering, Southeast University, Nanjing 210096, China³ School of Civil Engineering, Shandong Jianzhu University, Jinan 250101, China

* Correspondence: sym511@126.com

Abstract: To investigate the shear capacity and failure mechanism of RC beams after fire exposure, fourteen full-scale beams without stirrups were tested at ambient temperature and after fire exposure. Three parameters, including the loading ratio, shear span-to-depth ratio and longitudinal reinforcement ratio, were considered in static load tests. The deterioration mechanism of the shear bearing capacity at the diagonal section of RC beams without stirrups after fire exposure was experimentally, numerically and theoretically revealed, and a calculation formula for the shear capacity of post-fire beams without stirrups was proposed. The results show that the shear capacity and stiffness of the specimens decreased after fire exposure, and the shear strength loss of the beams increased with fire exposure time. The shear capacity and stiffness of fire-damaged specimens decreased as the shear span ratio λ increased, and the shear strength loss of the beams decreased with λ . Compared with the theoretical calculation and experimental results of beams without stirrups, the average of the absolute errors was 10.48%. Therefore, this formula can better calculate the residual shear capacity of beam without stirrups after fire exposure.

Keywords: fire exposure; shear capacity; shear span ratio; load ratio; longitudinal reinforcement ratio



Citation: Song, Y.; Fu, C.; Liang, S. Residual Shear Capacity of RC Beams without Stirrups after Fire Exposure. *Buildings* **2022**, *12*, 1706. <https://doi.org/10.3390/buildings12101706>

Academic Editor: Elena Ferretti

Received: 16 August 2022

Accepted: 16 September 2022

Published: 17 October 2022

Publisher's Note: MDPI stays neutral with regard to jurisdictional claims in published maps and institutional affiliations.



Copyright: © 2022 by the authors. Licensee MDPI, Basel, Switzerland. This article is an open access article distributed under the terms and conditions of the Creative Commons Attribution (CC BY) license (<https://creativecommons.org/licenses/by/4.0/>).

1. Introduction

When a fire occurs in a building, the high temperature can seriously degrade the bearing capacity of reinforced concrete (RC) members. The internal force and stress redistribution resulting from the high temperature can have a complex impact on the shear bearing capacity of the RC members. The bearing safety of the diagonal section of members after fire exposure should be of great concern, and the steel bars affected by the high temperature should be strengthened. It is thus urgent to accelerate research on the shear bearing capacity of beams exposed to fire.

Xiao et al. [1] analysed the effects of high temperature on the strength and deflection of concrete, focused on the differences in fire resistance between ordinary concrete and high-strength concrete, and systematically studied the phenomenon and mechanism of concrete bursting after fire exposure. Zhang et al. [2] assessed the performance of RC structures under high temperature and put forward effective suggestions on how to carry out effective structural repair and reinforcement. Jiang et al. [3] conducted the shear tests on twenty-five beams to study the difference in their shear performance before and after fire exposure, and developed a simplified evaluation process to evaluate the shear capacity of RC beams after fire. Xing et al. [4] carried shear load tests on seven beams to investigate the effect of shear span ratio and heating positions on shear behavior of beams, and presented a simplified approach for evaluating the residual shear strength. Higuchi et al. [5] studied experimentally the remaining shear capacity of high strength RC members to confirm resilience after high temperature rise to 1000 °C degrees or more, and proposed the measures to protect the fixing parts from damage. Fu et al. [6,7] analysed

the temperature field distribution of RC frame joints and RC beams under the standard ISO 834 temperature curve. Liu et al. [8] studied the failure mode of reinforced concrete beams with carbon fibre cloth exposed to fire. Lie et al. [9,10] conducted an experimental study on the properties of reinforced concrete compression-bending members under high temperature. El-Hawary et al. [11,12] conducted fire tests of eight reduced-scale beams and analysed the effects of fire time and concrete protective thickness on the ultimate bearing capacity of the beams.

Although the behaviours of RC beams subjected to high temperature have been studied by many researchers, studies on the failure mechanism and shear capacity of RC members exposed to fire are still very limited. The shear properties of fire-damaged RC beams were studied on the basis of beams without stirrups. Fourteen full-scale RC beams without stirrups were designed, considering the effects of the loading ratio, fire exposure time, shear span ratio and longitudinal reinforcement ratio on the shear capacity of RC beams. The RC beams were exposed to three-sided fire conditions with the standard ISO 834 temperature curve [13]. Based on the ABAQUS finite element analysis (FEA) software [14], a numerical analysis method of RC beams after fire exposure was established, and the accuracy of this method was verified according to the experimental results. Based on this FEA method, the shear span ratio, fire time, and longitudinal reinforcement ratio were selected as critical parameters to study the shear performance of forty-eight beams without stirrups, and a shear capacity calculation formula of post-fire beams without stirrups was proposed.

2. Experimental Tests

2.1. Test Specimens

To investigate the shear capacity of an RC beam without stirrups after fire exposure, fourteen full-scale RC beams without stirrups were fabricated: one was unfired and employed as a reference, and the others were fired according to the size of the furnace chamber ($9000 \times 4500 \times 1500$ mm). The length of the beams was 4000 mm, and the cross-section and reinforcement details of all beams are presented in Figure 1 and Table 1. The specimens were designed according to ‘strong bending and weak shear’ following the Chinese design code [15]. The cover thickness to the longitudinal reinforcement for all beams was kept at 25 mm. Stirrups were placed in the beam ends. The tested yield strengths f_y of C20 and C25 for longitudinal reinforcement were 413 MPa and 451 MPa, respectively. The tested average compressive strength of the three concrete cubes ($150 \times 150 \times 150$ mm) was 31.6 MPa. In the names of the specimens, ‘NBH’ indicates that the specimen was not subjected to fire, while those without ‘N’ were subjected to fire. ‘ P_u ’ indicates the ultimate load bearing capacity of the beam at ambient temperature, and ‘ ρ ’, ‘ λ ’, ‘ t ’ and ‘ δ ’ indicate the longitudinal reinforcement ratio, shear span ratio, fire time and load ratio at high temperature, respectively.

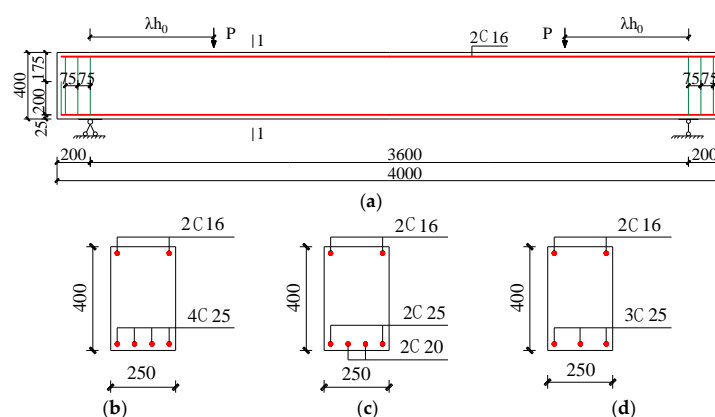


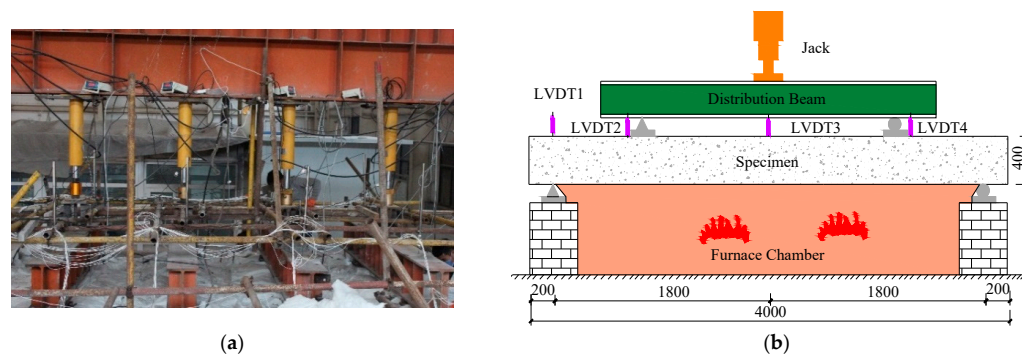
Figure 1. The cross-section and reinforcement details of beams (in mm). (a) Scheme of beams. (b) $\rho = 1.96\%$ (c) $\rho = 1.61\%$ (d) $\rho = 1.47\%$.

Table 1. Design parameters of specimens.

Specimens	Cross-Section Size/mm	Longitudinal Reinforcement Ratio $\rho\%$	Shear Span Ratio λ	Fire Time t/min	Load Ratio δ
NBH1	250 × 400	1.96	2.1	0	/
BH1	250 × 400	1.96	2.1	60	/
BH2	250 × 400	1.96	2.1	90	/
BH3	250 × 400	1.96	2.1	90	0.4 P_u
BH4	250 × 400	1.96	2.1	120	/
NBH2	250 × 400	1.96	2.6	0	/
BH5	250 × 400	1.96	2.6	90	/
BH6	250 × 400	1.96	2.6	90	0.4 P_u
NBH3	250 × 400	1.96	3.3	0	/
BH7	250 × 400	1.96	3.3	90	/
NBH4	250 × 400	1.61	2.1	0	/
BH8	250 × 400	1.61	2.1	90	/
NBH5	250 × 400	1.47	2.1	0	/
BH9	250 × 400	1.47	2.1	90	/

2.2. Test Setup and Instrumentation

After curing, the beams were transferred to a furnace chamber for heating following the temperature curve prescribed by standard ISO 834 [13], as shown in Figure 2a. The underside and two sides of the beams were fabricated in the furnace, as illustrated in Figure 2b. Before heating, the load was first added to the applied load. After the load stabilized, the heating began. This load was kept constant during the fire test, and the general arrangement of the test setup is shown in Figure 3. Four thermocouples were installed along the furnace length to monitor the temperature of the furnace. To calibrate the temperature distribution under fire exposure, a series of K-type thermocouples were installed in the cross-section of beams, as shown in Figure 4. After reaching the set fire time, the furnace chamber was switched off, and fire-damaged beams were allowed to cool down naturally to room temperature.

**Figure 2.** Layout of the fire test. (a) The furnace chamber (b) Specimen arrangement in the furnace.**Figure 3.** Fire test setup (dimensions in mm). (a) Vertical load (b) Location of LVDTs.

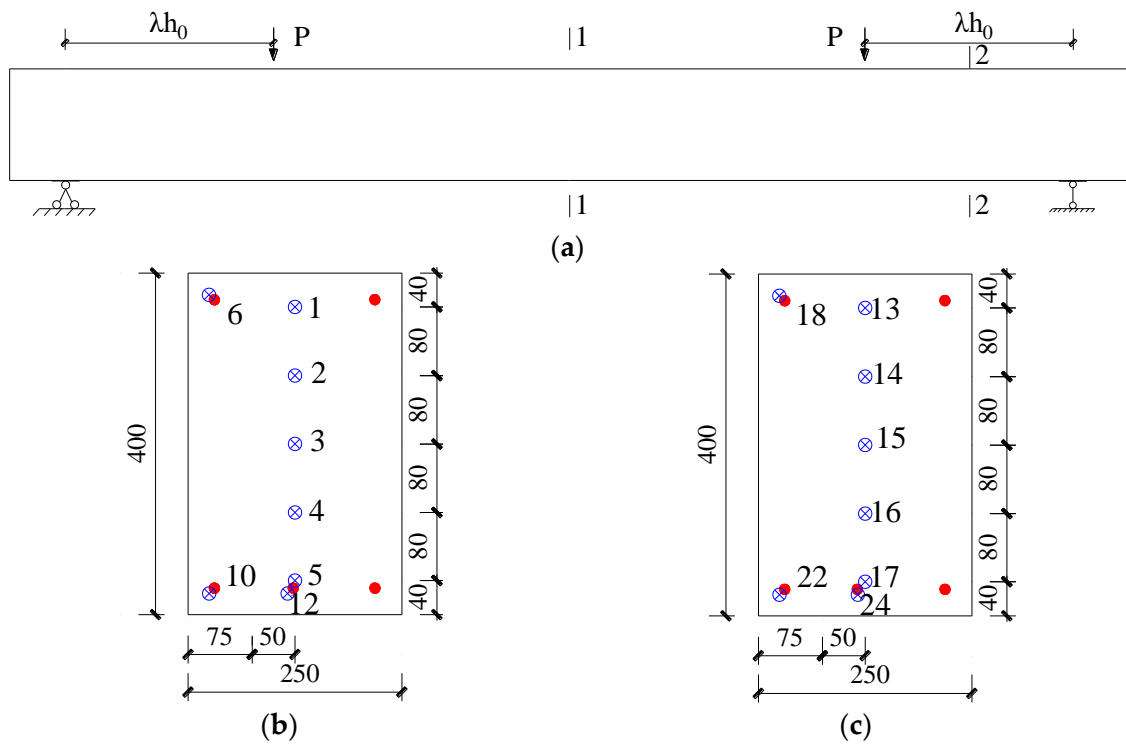


Figure 4. Location of thermocouples (dimensions in mm). (a) Location of thermocouples (b) 1–1 section (c) 2–2 section.

A schematic diagram of the static load test setup, strain gauges and linear displacement transducers (LVDTs) are shown in Figure 5.

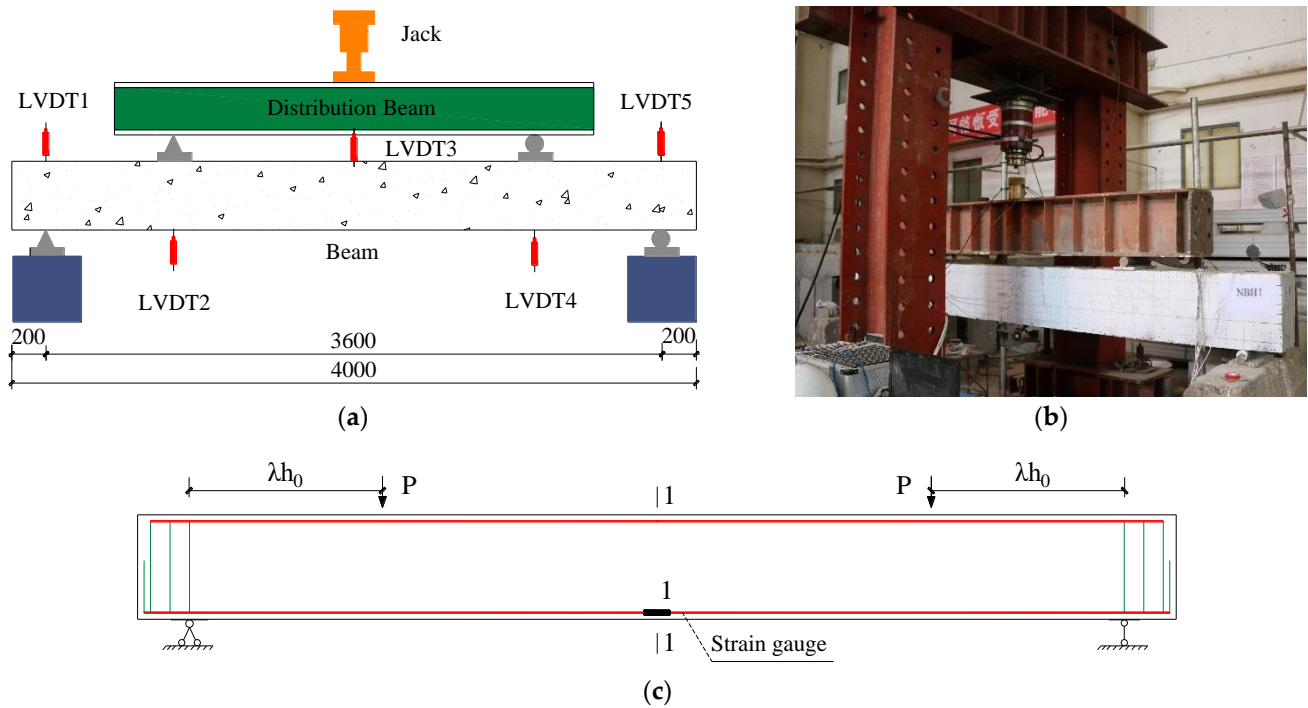
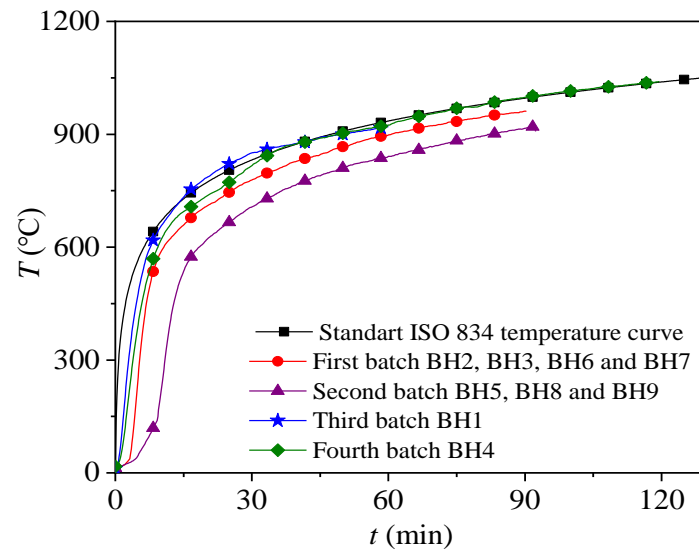


Figure 5. The static load test setup (dimensions in mm). (a) Configuration of the test setup (b) Beam during the test (c) Location of the strain gauges.

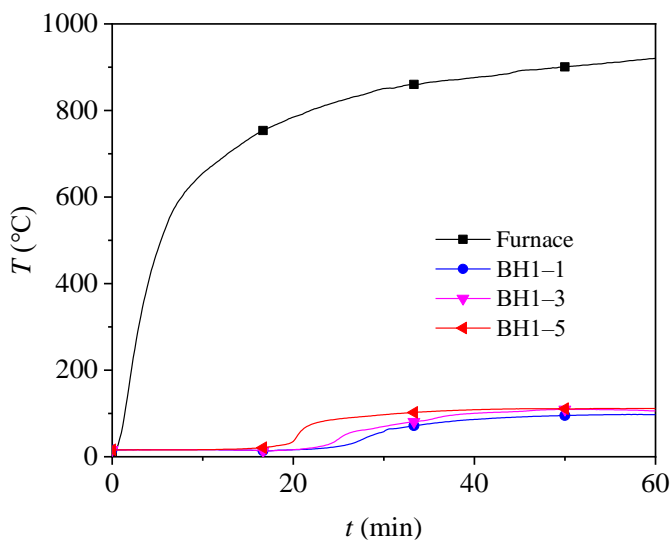
3. Experimental Results and Discussion

3.1. Thermal Response

Figure 6 shows the temperature at various locations inside the beam and the furnace. Strict temperature control according to ISO 834 could not be conducted due to the limitations of the furnace equipment. For the furnace temperature, the average of the four thermocouples installed along the length of the furnace is reported, as shown in Figure 6a. It is evident that the furnace temperature was lower than the ISO 834 temperature [13]. In an electric furnace, heating is applied along three faces, and the temperature difference between the bottom and top of the beam is large, resulting in an uneven temperature distribution. With increasing section height, the temperature of the measuring point decreases; that is, the temperature is related to the distance from the fire surface, and the temperature increases with decreasing distance from the fire surface.



(a)



(b)

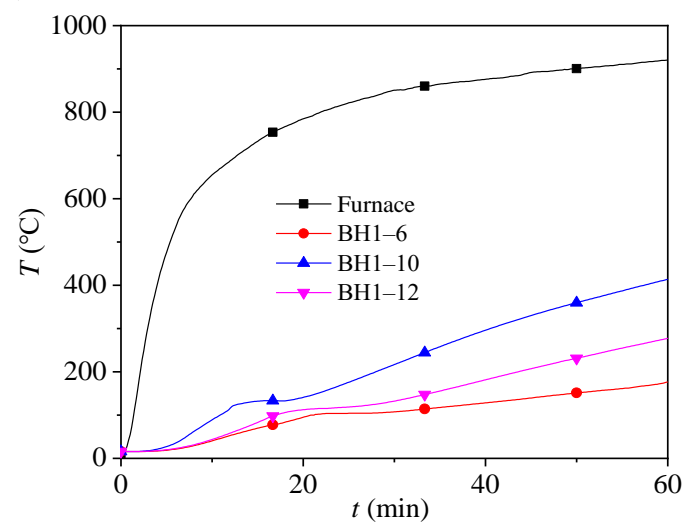


Figure 6. Cont.

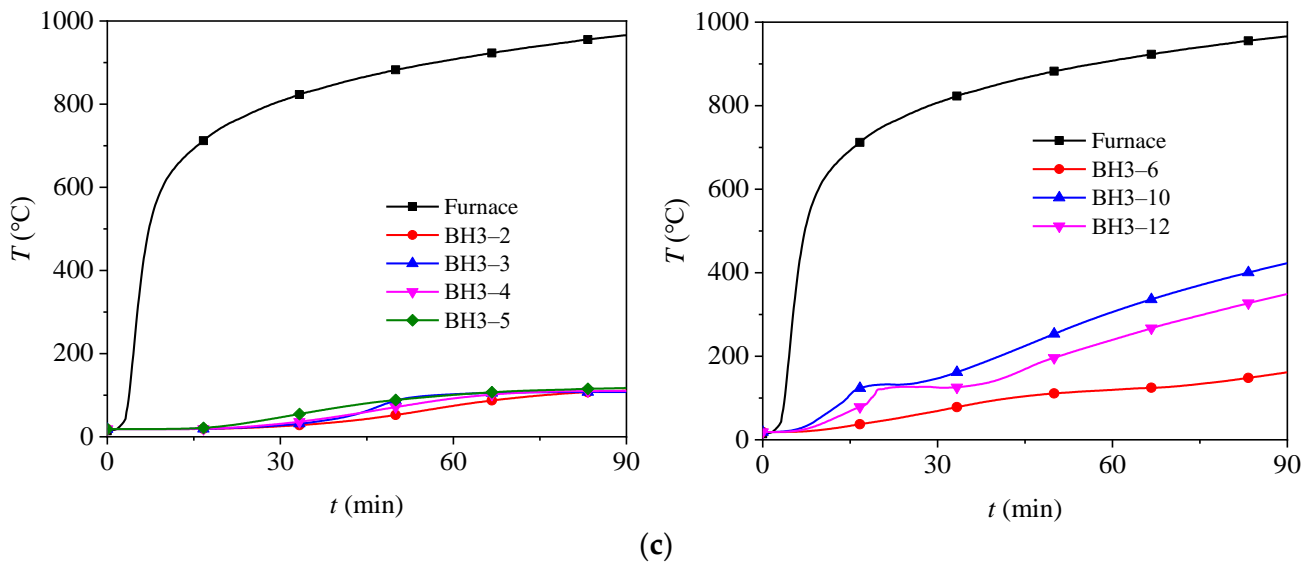


Figure 6. Temperature–time curves of beams. (a) Temperature–time curve in the furnace. (b) Temperature–time curve of BH1. (c) Temperature–time curve of BH3.

3.2. Structural Responses

3.2.1. Failure Modes

Considering the large number of beams, only the failure modes and crack distributions of the partial beams in the static load test are illustrated in Figure 7 for simplicity, where the red lines in Figure 7 is the main crack of beams. The final failure mode of all beams was shear failure. Compared with the beam at ambient temperature, the beams exposed to high temperature generated many more and wider cracks. In addition, the distribution of diagonal cracks was more extensive in the shear-bending zone.

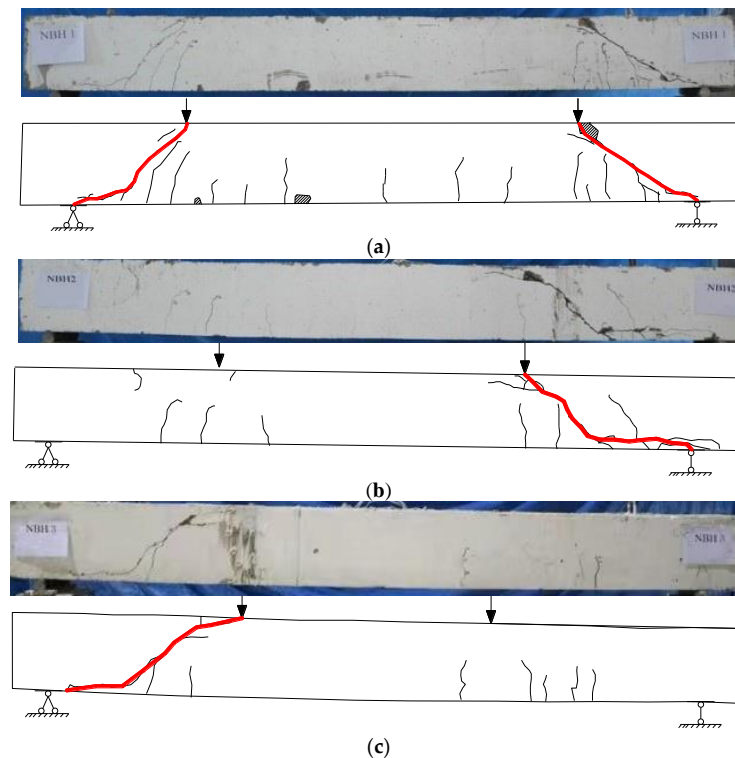


Figure 7. Cont.

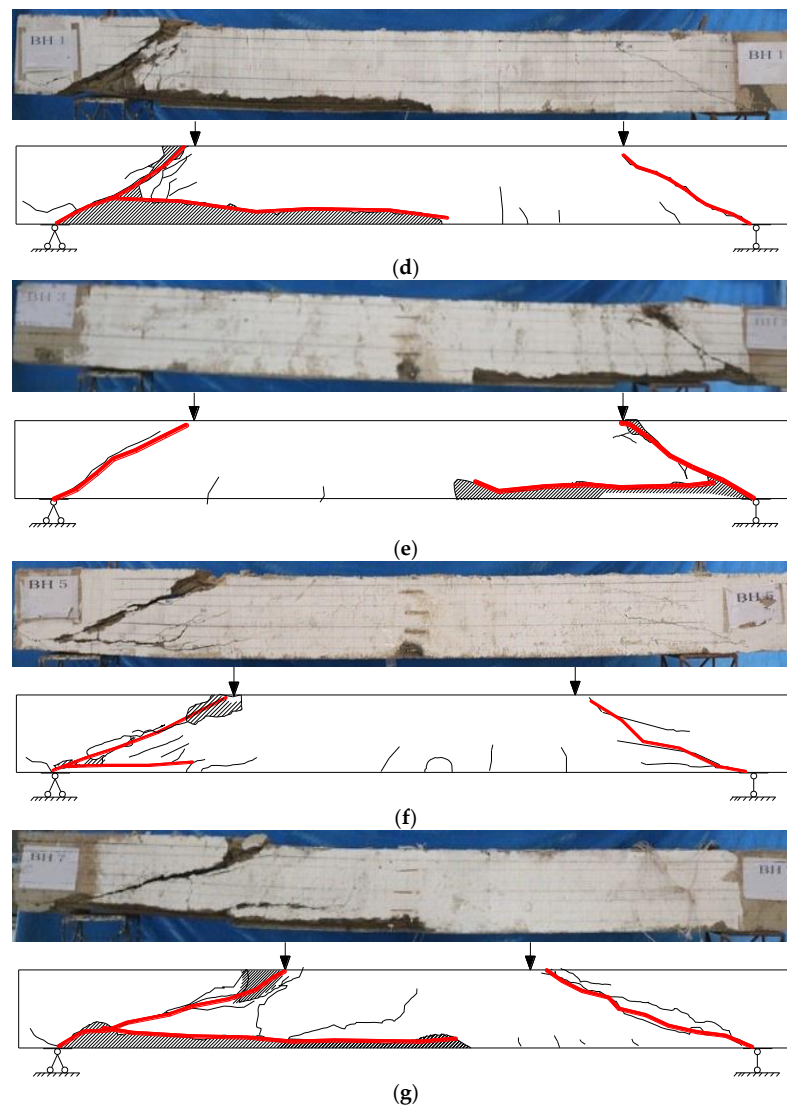


Figure 7. Diagonal cracks in beams resulting in their ultimate destruction. (a) NBH1 (b) NBH2 (c) NBH3 (d) BH1 (e) BH3 (f) BH5 (g) BH7.

3.2.2. Shear Capacity of Specimens

The output load of the hydraulic jack, the occurrence of flexural and diagonal cracks, and the strains of longitudinal reinforcements were presented simultaneously during the loading procedure. The ultimate shear load P_u and shear cracking load P_{cr} are listed in Table 2. For a simply supported beam, the load value in the Table 2 is the one-point load value. the following conclusions can be obtained:

1. The shear capacity of the specimens without stirrups decreased after fire exposure, as shown in Figure 8. For instance, compared with the specimen NBH1 at room temperature, the shear bearing capacity of BH1 decreased by 10.5%. The shear strength loss of beams increased with increasing fire exposure time t , such as those of BH1, BH2 and BH4 (10.5% < 24.7% < 36.8%). The relationship between the residual shear capacity and fire time t is shown in Equation (1), where ' P_{uT} ' and ' P_u ' indicate the ultimate load bearing capacity of the beam after fire exposure and at room temperature, respectively.

$$P_{uT} = (1.23 - 0.38t + 0.04t^2)P_u \quad (1)$$

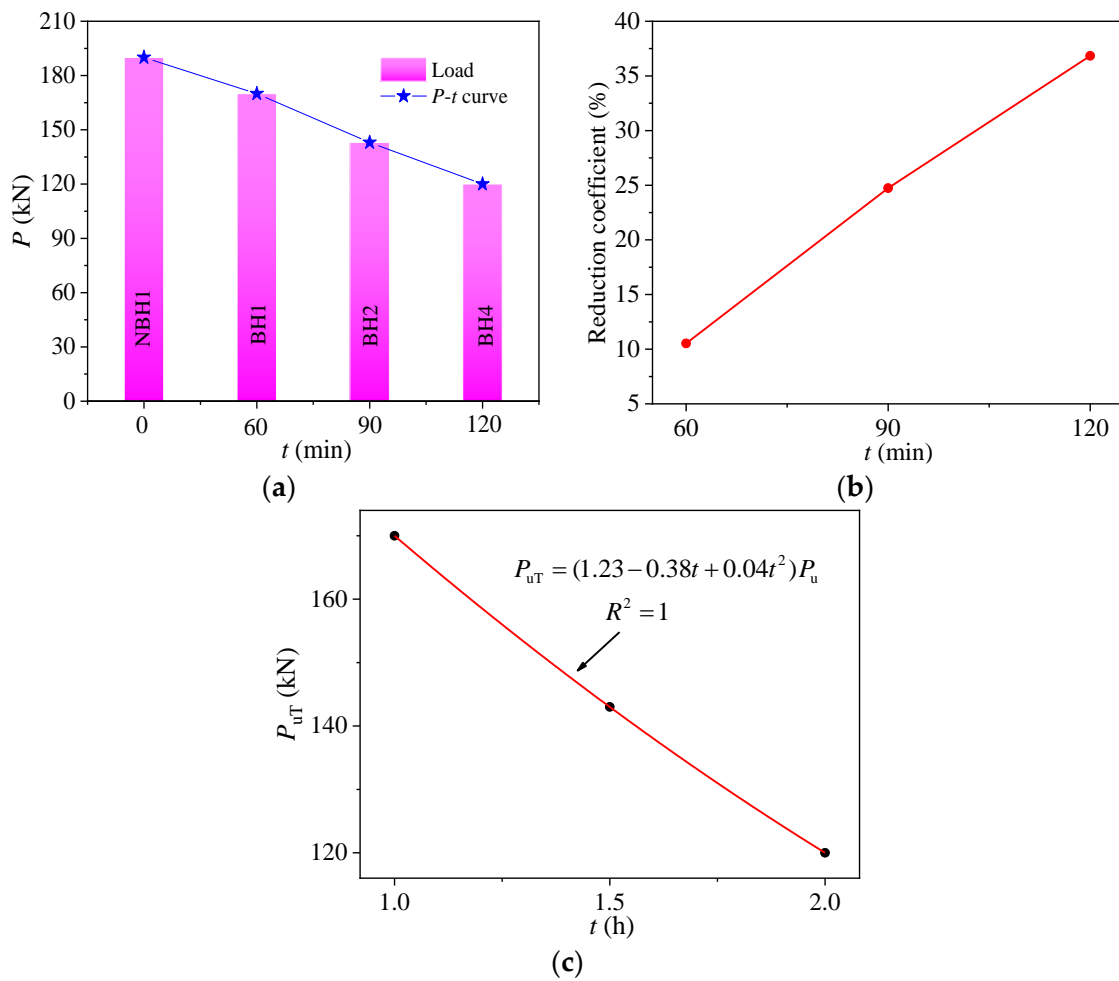


Figure 8. The effect of t on the residual shear capacity of beams. (a) Residual shear capacity (b) Reduction coefficient of shear strength (c) The relationship of P_{uT} vs. t .

Table 2. Shear capacity of beams without stirrups.

No.	$\rho_{sv}/\%$	$\rho/\%$	λ	t/min	δ	P_{cr}/kN	P_u/kN	f/mm
NBH1	0.00	1.96	2.1	0	/	50	190	13.12
BH1	0.00	1.96	2.1	60	/	50	170	15.35
BH2	0.00	1.96	2.1	90	/	40	143	14.22
BH3	0.00	1.96	2.1	90	0.4	0	80	9.09
BH4	0.00	1.96	2.1	120	/	40	120	15.55
NBH2	0.00	1.96	2.6	0	/	35	175	9.72
BH5	0.00	1.96	2.6	90	/	50	140	18.06
BH6	0.00	1.96	2.6	90	0.4	40	98.5	9.81
NBH3	0.00	1.96	3.3	0	/	50	140	11.72
BH7	0.00	1.96	3.3	90	/	40	115	15.63
NBH4	0.00	1.61	2.1	0	/	60	180	12.22
BH8	0.00	1.61	2.1	90	/	40	138	15.23
NBH5	0.00	1.47	2.1	0	/	60	170	11.46
BH9	0.00	1.47	2.1	90	/	50	120	16.62

- The shear capacity of fire-damaged specimens decreased with increasing preload, such as those of BH2 and BH3 (143 kN > 80 kN), BH5 and BH6 (140 kN > 98.5 kN), as shown in Table 2. Compared with residual shear capacity of no preloaded beam BH2 and BH5, that of thermo-mechanical beams BH3, BH6 is reduced by 44.1% and 29.6%, respectively. Therefore, the residual shear capacity degradation of beams

under the coupling of fire and constant load was higher than that of beams only under fire without constant load. That is, the shear capacity of beams undergoing thermo-mechanical coupling could be further degraded.

- The shear capacity of specimens exposed to fire decreased with increasing λ , such as those of BH2, BH5 and BH7 (143 kN > 140 kN > 110 kN), which is consistent with that of the specimen at ambient temperature, as shown in Figure 9. The shear strength loss of the beams decreased with increasing shear span ratio λ , such as those of BH2, BH5 and BH7 (24.7% > 20.0% > 17.8%). The relationship between the residual shear capacity and shear span ratio λ is shown in Equation (2).

$$P_{uT} = \frac{6.90}{\lambda + 2.16} bh_0 \quad (2)$$

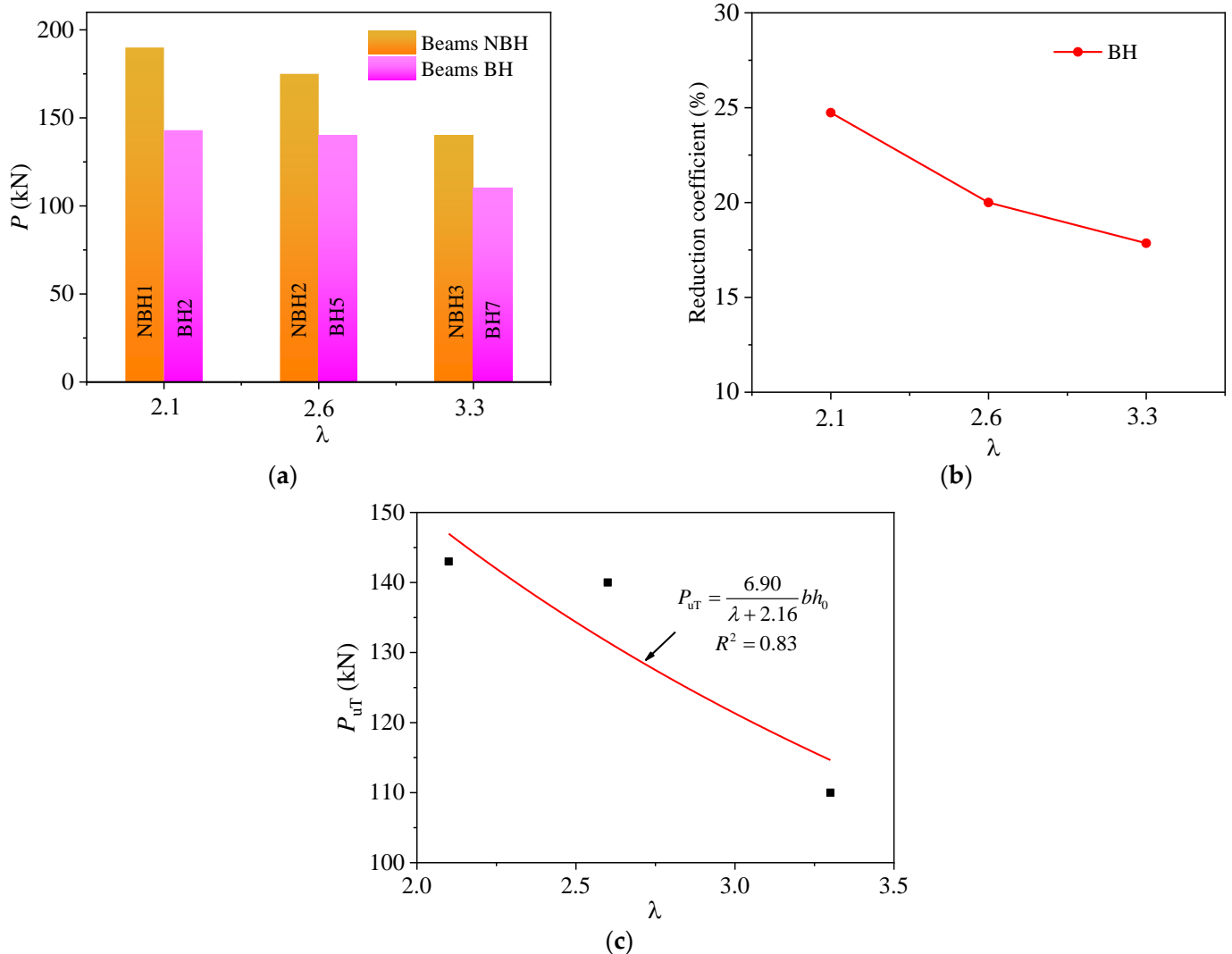


Figure 9. The effect of λ on the residual shear capacity P of beams. (a) Residual shear capacity (b) Reduction coefficient of shear strength (c) Relationship of P_{uT} vs. λ .

- The shear capacity of fire-damaged specimens increased as the longitudinal reinforcement ratio ρ increased, such as those of BH2, BH8 and BH9 (143 kN > 138 kN > 120 kN), which is consistent with that of the specimen at ambient temperature, as shown in Figure 10. The shear strength loss of the beams increased as the longitudinal reinforcement ratio ρ increased, such as those of BH2, BH8 and BH9 (24.7% > 12.2% > 8.8%).

The relationship between the residual shear capacity and longitudinal reinforcement ratio ρ is shown in Equation (3).

$$P_{uT} = 1.13\rho^{0.51}bh_0 \quad (3)$$

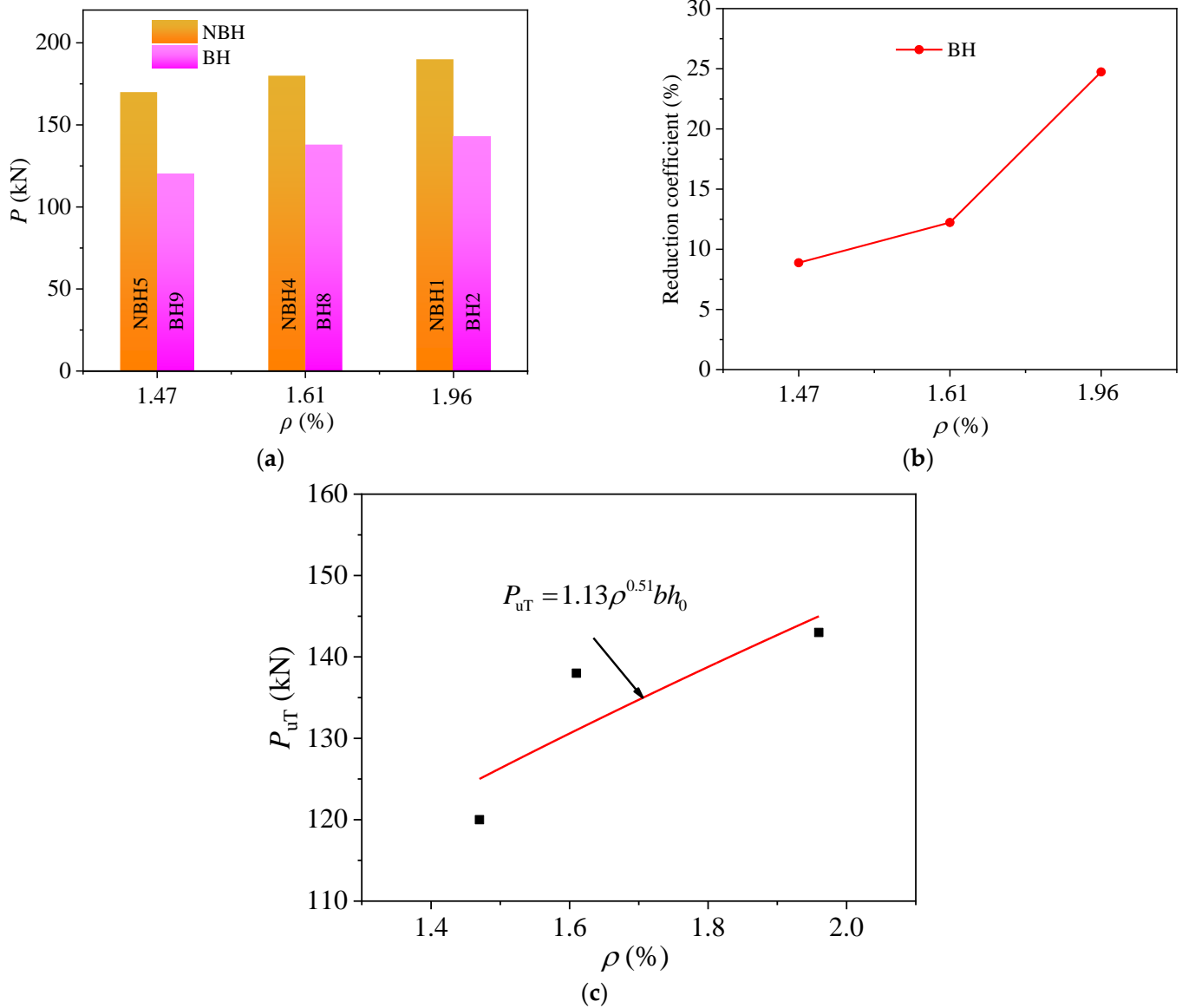


Figure 10. The effect of ρ on the residual shear capacity P of beams. (a) Residual shear capacity (b) Reduction coefficient of shear strength (c) Relationship of P_{uT} vs. ρ .

Combined with the test results, considering the relationship of the residual shear capacity P_{uT} , shear span ratio λ and longitudinal reinforcement ratio ρ on beams after high temperature, by fitting the data in Table 2, the three-dimensional relationship of P_{uT} , λ and ρ of post-fire beams without stirrups is shown in Figure 11, and its expression is shown in Equation (4).

$$P_{uT} = 1.98\left(\frac{\rho}{\lambda}\right)^{1.17}bh_0 \quad (4)$$

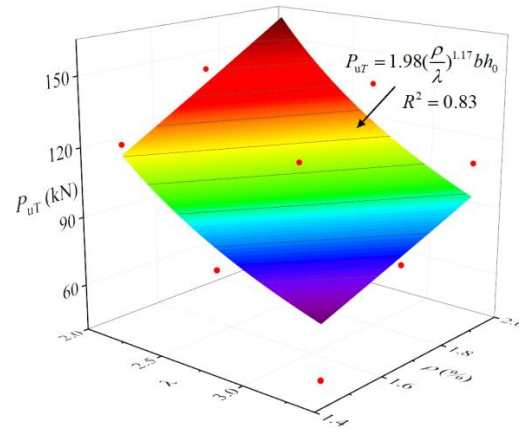


Figure 11. The three-dimensional relationship between P_{uT} , λ and ρ .

3.2.3. Specimen Stiffness

The load–deflection curves of different specimens are shown in Figure 12. By analyzing these curves, the following conclusions can be obtained:

1. Both the shear capacity and the stiffness of post-fire beams without stirrups declined.
2. Figure 12a,b,d show that the stiffness of the specimens decreased as the fire exposure time (t), shear span ratio (λ) and load ratio (δ) increased.
3. Figure 12c shows that the stiffness of the specimens increased with increasing longitudinal reinforcement ratio ρ .

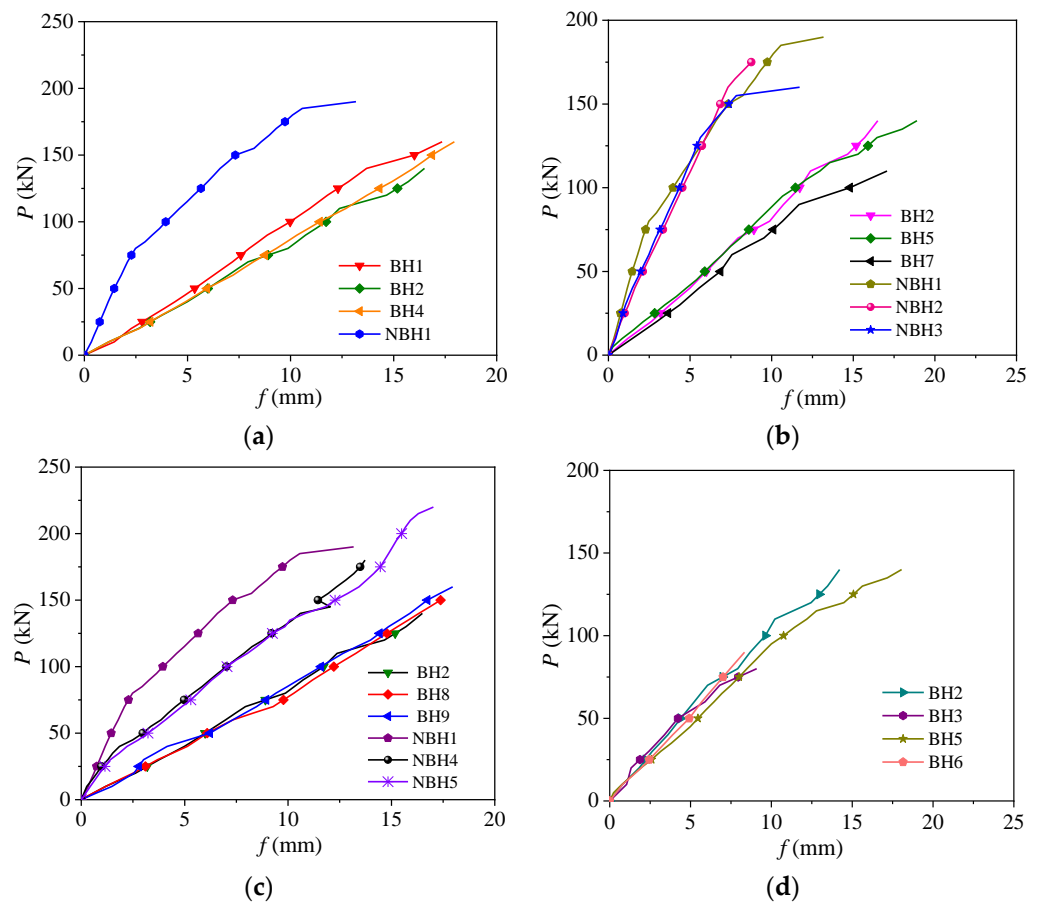


Figure 12. The load–vertical displacement curves of various specimens. (a) Fire exposure time t (b) Shear span ratio λ (c) Longitudinal reinforcement ratio ρ (d) Load ratio.

3.2.4. Strain Distribution

Figure 13 shows the load–strain curves of the post-fire specimens. Strain gauges were attached to the longitudinal reinforcement to measure the strains at the mid-span section. For all the specimens, the strain in the longitudinal reinforcement did not reach the yield value because all specimens failed due to the major shear cracking, as shown in Figure 13b.

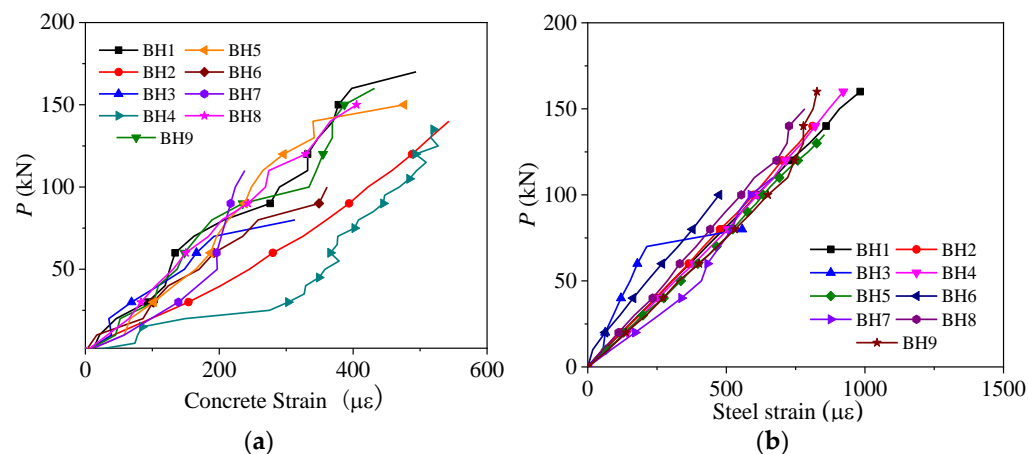


Figure 13. The load–strain curves of various specimens after fire exposure. (a) Concrete strain (b) Steel strain.

4. Finite Element Analysis

There are two methods used to evaluate the damage of concrete after fire exposure: (1) to obtain the fire damage directly through field tests; (2) to evaluate the extent of the damage to the section by numerical simulations or a simplified method. Finite element analysis can be used to supplement the deficiencies of experimental research in quantity and micro observation.

The finite element (FE) software package ABAQUS [14] was used to realize the proposed FE model. The constitutive models for concrete and steel were defined within the framework for the software package; the modelling of RC beams exposed to fire was undertaken using the sequentially coupled thermomechanical procedure. In this procedure, the mechanical analysis depends on the heat transfer analysis, but no reverse dependency exists. Therefore, the FE analysis included two steps: (1) a heat transfer analysis of the RC beam exposed to fire and (2) a mechanical analysis based on the heat transfer analysis

4.1. Heat Transfer Analysis

To clarify the effect of the shear span ratio, fire exposure time and longitudinal reinforcement ratio on the shear capacity of RC beams without stirrups after high temperature, the FE software package ABAQUS [14] was used to simulate the existing specimens. Figure 14 shows a configuration of the specimen's FE model, whose size and reinforcement are consistent with the previous tested specimen, as shown in Figure 1. In this FE model, the concrete and reinforcement framework are associated by using the surface-based tie constraint provided in ABAQUS, and the rectangular specimen shown in Figure 14 is exposed to fire on three surfaces.

For surfaces subjected to high temperature, the convective heat transfer coefficient is assumed to be a constant of $25 \text{ W}/(\text{m}\cdot\text{K})$, and the thermal emissivity is suggested to be 0.7 [16]. For the surfaces without fire, the convective heat transfer coefficient is assumed to be a constant of $9 \text{ W}/(\text{m}\cdot\text{K})$. For the whole model, the Stefan–Boltzmann constant is assumed to be $5.67 \times 10^{-8} \text{ W}\cdot\text{m}^{-2}\cdot\text{K}^{-4}$.

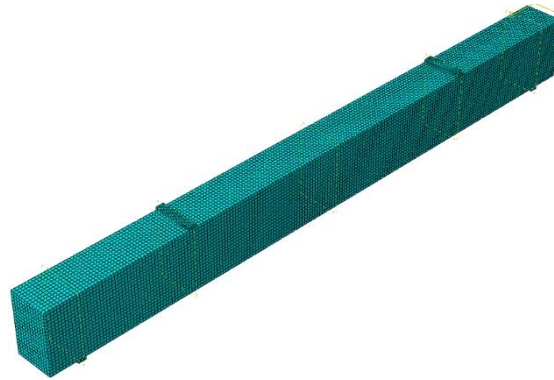


Figure 14. The FE model.

The thermal properties of concrete and steel, including the density, specific heat capacity, and heat conductivity, have been well investigated in previous research [17–20]. The density and specific heat capacity of the concrete and steel can be determined according to Eurocode 2 [17], and the heat conductivity of the concrete and steel is defined according to Lie [18]. The temperature rise curve used in the simulation is the measured temperature rise curve of the fire test, as shown in Figure 6. Figure 15 shows the temperature distribution of the beam under FE model.

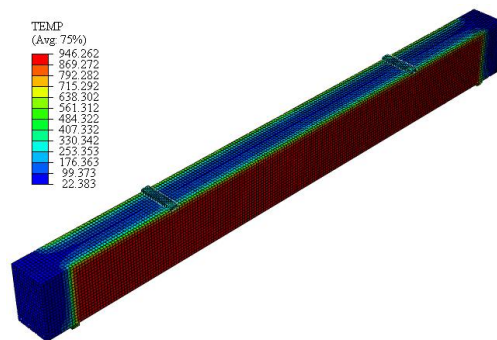


Figure 15. The temperature field distribution of the beam.

4.2. Mechanical Response Analysis

During the mechanical response analysis, the FE mesh remained the same as that used in the preceding heat transfer analysis, but the thermal elements were replaced with stress elements, which were eight-node continuum elements with reduced integration (C3D8R) for concrete and two-node link elements (T3D2) for the reinforcing steel. The total fire exposure period was divided into small time steps to ensure numerical convergence even for a highly nonlinear problem.

During the mechanical response analysis, the constitutive models of concrete and reinforcement are the main contents [21–25], and the concrete [21,22] is assigned the concrete damaged plasticity (CDP) constitutive model in ABAQUS. In the mechanical calculation, because the concrete adopts a solid element with continuity, which is not suitable for cracking and complex mechanical properties, ABAQUS/Explicit can be used for explicit dynamic analysis, and concrete cracking and crushing can be realized through element deletion. The contact constraint is set in the whole model, the interface friction coefficient is 0.3, and the interface normal direction adopts hard contact.

4.3. Validation of the FE model

The thermal performance coefficients of concrete and reinforcement and the mechanical properties of materials after high temperature are reasonably selected, the thermal

mechanical coupling model of the concrete beam after high temperature is established, and the model is verified by the experimental results, as shown in Figures 16 and 17.

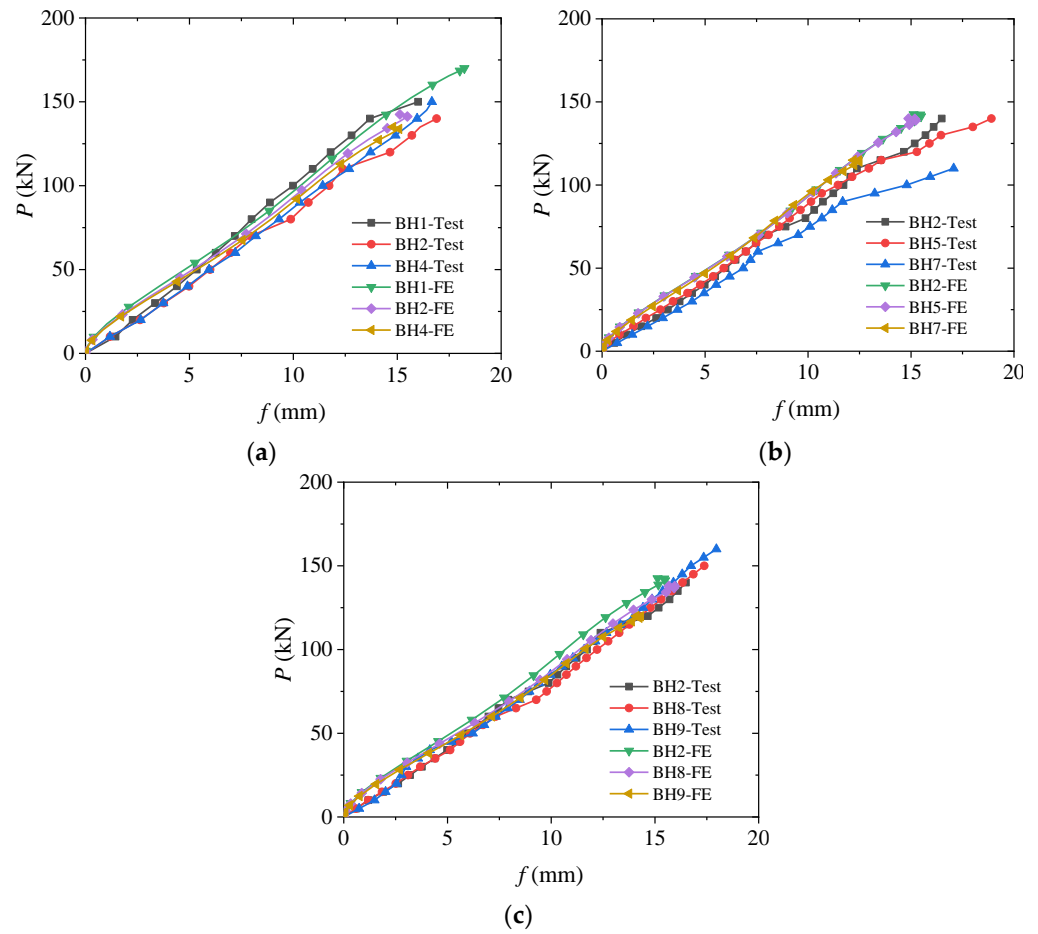


Figure 16. Comparison of load–vertical displacement curves for beams. (a) Fire time (b) Shear span ratio (c) Longitudinal reinforcement ratio.

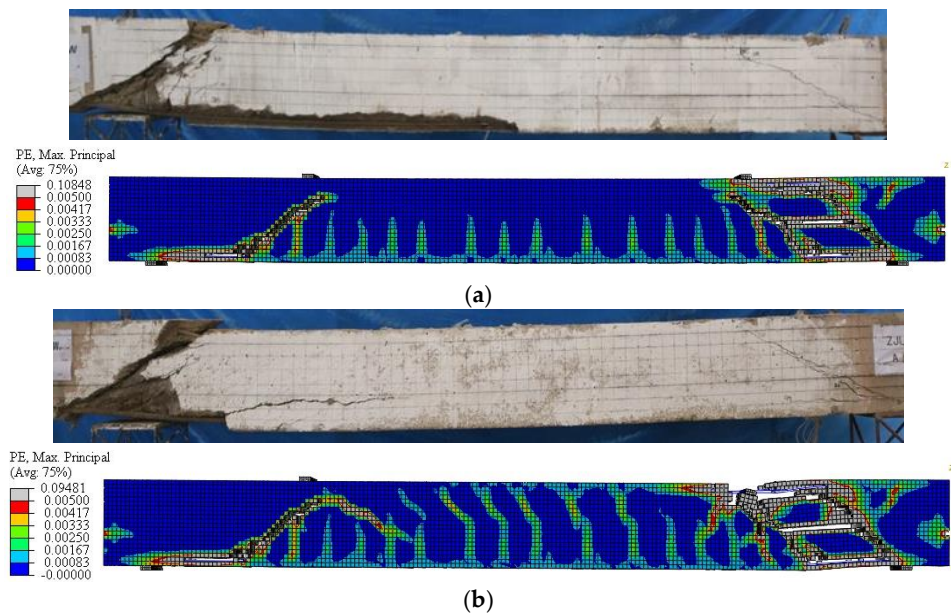


Figure 17. Cont.

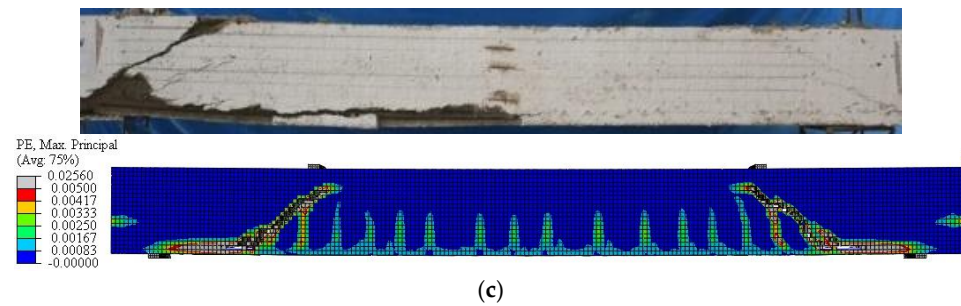


Figure 17. Failure model of the FE results and test results for the beams. (a) BH1 (b) BH2 (c) BH4.

5. Evaluation of the Residual Shear Capacity

There are several models for calculating shear strength of beams. Most of the suggested models were established through the regression analysis of the experimental data. Compared with the above experimental studies, the relationship between various parameters and the shear strength of beam without stirrups after fire exposure is mainly related to fire exposure time, the shear span ratio, concrete strength, cross-section size, longitudinal reinforcement ratio and so on.

Zsutty [26] proposed a simple model using dimensional and statistical regression analysis to estimating the shear strength of beams without stirrups, as shown in Equation (5).

$$v_u = 2.2 \left(\frac{f'_c \rho}{\lambda} \right)^{1/3} b h_0 \quad (5)$$

The cylinder's compressive strength f'_c is directly proportional to the axial compressive strength f_c , which can be calculated by the conversion coefficient. Therefore, Equation (6) was suggested, which provided a reasonable estimate of the shear capacity of beams without stirrups:

$$v_u = \alpha \left(\frac{f_c \rho}{\lambda} \right)^\beta b h_0 \quad (6)$$

Based on the experimental and numerical analysis, taking shear span ratio λ , fire time t and longitudinal reinforcement ratio ρ as the parameters, the above numerical simulation method was used to carry out a parametric expansion analysis of the beams without stirrups after high temperature, and the influence of various parameters on the residual shear capacity of postfire beams without stirrups are studied. The temperature rise is controlled by the standard ISO 834 temperature curve [13]. The specimen shows obvious shear failure in the shear-bending area. The simulation results are shown in Table 3.

Table 3. Shear capacity of beams without stirrups under different fire times.

No.	t/min	λ	$\rho/\%$	P_u/kN
B1	0	1.0	1.47	301.47
B2	0	1.0	1.96	320.31
B3	0	1.5	1.47	234.34
B4	0	1.5	1.96	282.63
B5	0	2.0	1.47	160.16
B6	0	2.0	1.96	179.79
B7	0	2.5	1.47	134.47
B8	0	2.5	1.96	150.73
B9	0	3.0	1.47	112.06
B10	0	3.0	1.96	121.03
B11	0	3.5	1.47	92.06
B12	0	3.5	1.96	104.62

Table 3. Cont.

No.	t/min	λ	$\rho/\%$	P_u/kN
B13	60	1.0	1.47	198.29
B14	60	1.0	1.96	208.20
B15	60	1.5	1.47	188.37
B16	60	1.5	1.96	193.33
B17	60	2.0	1.47	148.85
B18	60	2.0	1.96	158.63
B19	60	2.5	1.47	116.54
B20	60	2.5	1.96	127.18
B21	60	3.0	1.47	92.06
B22	60	3.0	1.96	108.34
B23	60	3.5	1.47	76.48
B24	60	3.5	1.96	96.25
B25	90	1.0	1.47	188.42
B26	90	1.0	1.96	178.46
B27	90	1.5	1.47	170.34
B28	90	1.5	1.96	173.26
B29	90	2.0	1.47	141.14
B30	90	2.0	1.96	158.63
B31	90	2.5	1.47	107.58
B32	90	2.5	1.96	126.54
B33	90	3.0	1.47	89.65
B34	90	3.0	1.96	94.89
B35	90	3.5	1.47	75.32
B36	90	3.5	1.96	89.50
B37	120	1.0	1.47	154.82
B38	120	1.0	1.96	158.63
B39	120	1.5	1.47	143.44
B40	120	1.5	1.96	149.83
B41	120	2.0	1.47	126.54
B42	120	2.0	1.96	143.76
B43	120	2.5	1.47	103.63
B44	120	2.5	1.96	126.54
B45	120	3.0	1.47	80.68
B46	120	3.0	1.96	94.19
B47	120	3.5	1.47	66.95
B48	120	3.5	1.96	77.87

Combined with the simulation results in Table 3, the relationship of the shear capacity, shear span ratio λ and longitudinal reinforcement ratio ρ for beams without stirrups under different fire times is shown in Figure 18.

The constants α and β for different fire times are given in Table 4. In order to propose a unified model for fire time t , the constants for their corresponding fire time are plotted in Figures 19 and 20. A polynomial trend-line is fitted for each constant, yielding an excellent R-squared value. Therefore, the constants α and β for the fire time t can be written in the following form:

$$\alpha = 1.13t^2 - 4.79t + 8.23 \quad (7)$$

$$\beta = 0.06t^2 - 0.29t + 0.83 \quad (8)$$

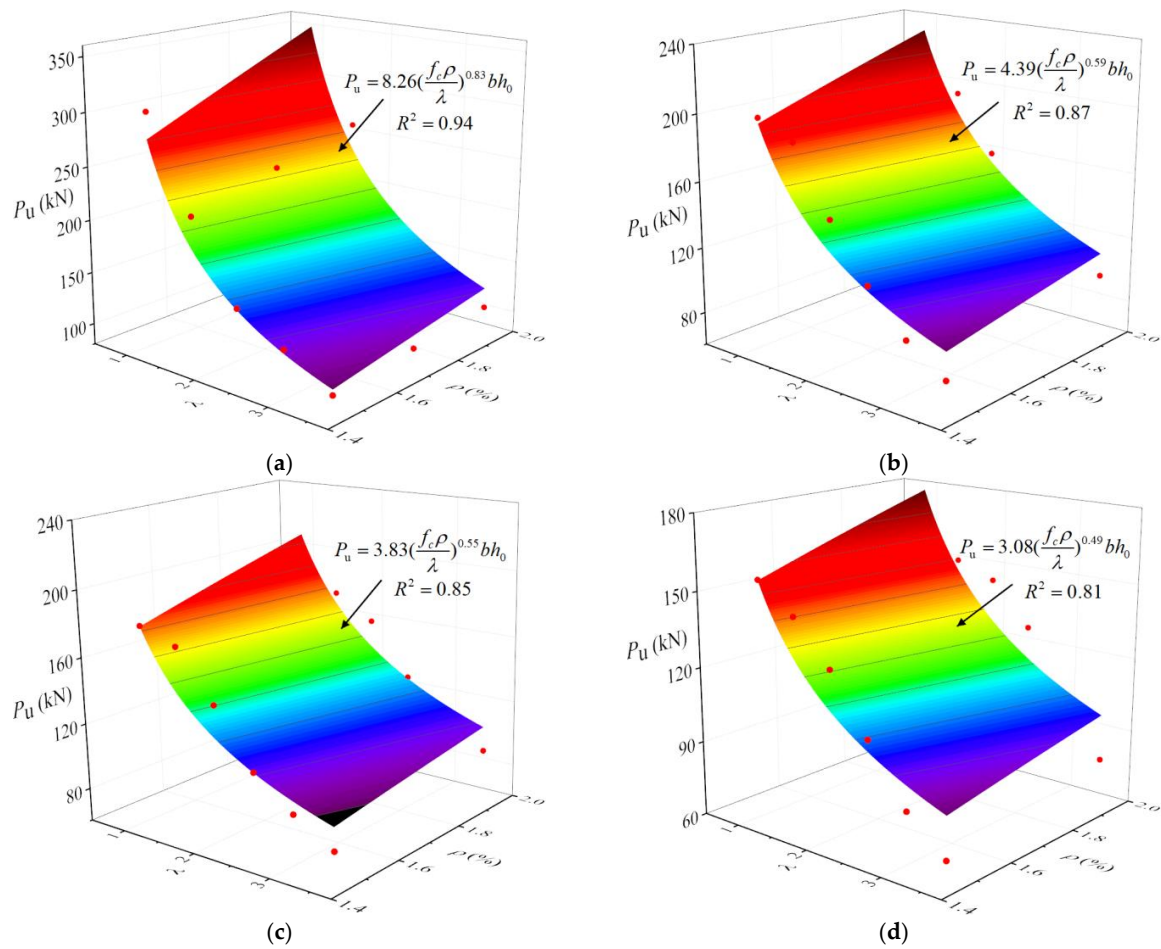


Figure 18. The relationship of P_u , λ and ρ for beams without stirrups under different fire times. (a) $t = 0$ min (b) $t = 60$ min (c) $t = 90$ min (d) $t = 120$ min.

Table 4. Values of α and β for different fire times.

t/h	α	β	R^2
0	8.26	0.83	0.94
1	4.39	0.59	0.87
1.5	3.83	0.55	0.85
2	3.08	0.49	0.81

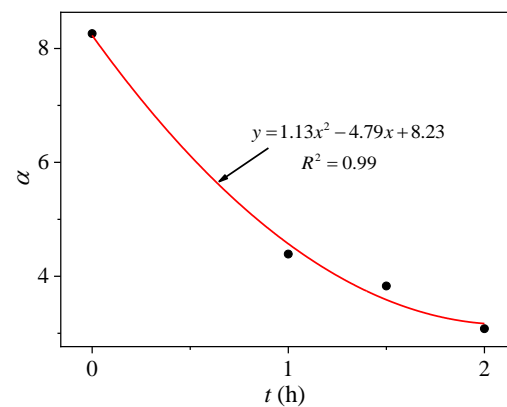


Figure 19. Variation of α with the fire time.

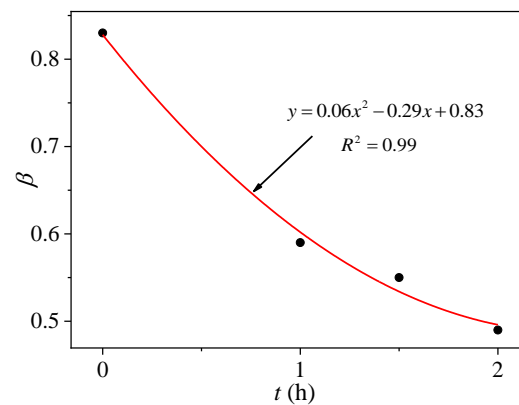


Figure 20. Variation in β with the fire time.

Generally, when the load value under high temperatures is small, the influence of the load under high temperatures can be ignored. When the load under high temperatures is large, the influence of the load value δ at high temperatures should be considered. The shear bearing capacity of a loaded beam under high temperature can be calculated by multiplying the shear bearing capacity without load under high temperature by the reduction coefficient [27,28], which can be expressed by the following formula:

$$\eta = (0.163\lambda - 0.584)\delta^3 + 1 \quad (9)$$

Therefore, the residual shear capacity of the RC beam without stirrups after fire time t can be expressed by Equation (10).

$$v_{uT} = ((0.163\lambda - 0.584)\delta^3 + 1)(1.13t^2 - 4.79t + 8.23)\left(\frac{f_c \rho}{\lambda}\right)^{(0.06t^2 - 0.29t + 0.83)} b h_0 \quad (10)$$

The shear capacities of all beams in the experimental and numerical studies were calculated using the simplified evaluation process, as shown in Table 5 and Figure 21, where V_{test} is judged by the results obtained from the analysis shown in Table 3 and the experimental results shown in Table 2, and V_{cal} is judged by the results obtained from the proposed formula. Comparing the calculation and the experimental results, the calculation values of the beam without stirrups after fire exposure is in good agreement with the experimental values, and the average absolute error is 10.48%. Although the test data are scattered to a certain degree and there are some differences between the calculation and experimental results, the calculation formula can still evaluate the shear capacity of beams without stirrups after fire with acceptable accuracy.

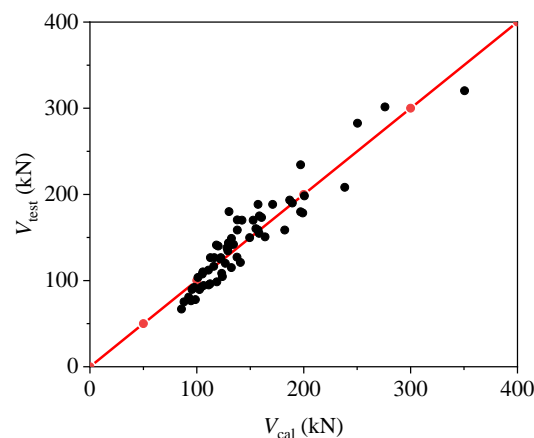


Figure 21. Comparison of V_{cal} and V_{test} for beams.

Table 5. Comparison between the theoretical and experimental values of the beams without stirrups.

Data Sources	No.	t/min	λ	$\rho/\%$	V_{test}/kN	V_{cal}/kN	$(V_{test} - V_{cal})/V_{test}/\%$
	B1	0	1.0	1.47	301.47	276.05	8.43
	B2	0	1.0	1.96	320.31	350.50	-9.42
	B3	0	1.5	1.47	234.34	197.16	15.86
	B4	0	1.5	1.96	282.63	250.34	11.42
	B5	0	2.0	1.47	160.16	155.28	3.04
	B6	0	2.0	1.96	179.79	197.16	-9.66
	B7	0	2.5	1.47	134.47	129.03	4.04
	B8	0	2.5	1.96	150.73	163.83	-8.69
	B9	0	3.0	1.47	112.06	110.91	1.02
	B10	0	3.0	1.96	121.03	140.82	-16.35
	B11	0	3.5	1.47	92.06	97.59	-6.01
	B12	0	3.5	1.96	104.62	123.91	-18.44
	B13	60	1.0	1.47	198.29	200.65	-1.19
	B14	60	1.0	1.96	208.20	238.45	-14.53
	B15	60	1.5	1.47	188.37	157.32	16.48
	B16	60	1.5	1.96	193.33	186.96	3.29
	B17	60	2.0	1.47	148.85	132.38	11.07
	B18	60	2.0	1.96	158.63	157.32	0.83
	B19	60	2.5	1.47	116.54	115.79	0.64
	B20	60	2.5	1.96	127.18	137.60	-8.19
	B21	60	3.0	1.47	92.06	103.79	-12.74
	B22	60	3.0	1.96	108.34	123.35	-13.85
	B23	60	3.5	1.47	76.48	94.62	-23.72
	B24	60	3.5	1.96	96.25	112.45	-16.83
Table 3	B25	90	1.0	1.47	188.42	170.96	9.27
	B26	90	1.0	1.96	178.46	199.12	-11.57
	B27	90	1.5	1.47	170.34	137.90	19.04
	B28	90	1.5	1.96	173.26	160.61	7.29
	B29	90	2.0	1.47	141.14	118.40	16.11
	B30	90	2.0	1.96	158.63	137.90	13.07
	B31	90	2.5	1.47	107.58	105.19	2.22
	B32	90	2.5	1.96	126.54	122.52	3.18
	B33	90	3.0	1.47	89.65	95.50	-6.53
	B34	90	3.0	1.96	94.89	111.23	-17.22
	B35	90	3.5	1.47	75.32	88.01	-16.85
	B36	90	3.5	1.96	89.50	102.51	-14.53
	B37	120	1.0	1.47	154.82	158.31	-2.25
	B38	120	1.0	1.96	158.63	182.27	-14.90
	B39	120	1.5	1.47	143.44	129.78	9.52
	B40	120	1.5	1.96	149.83	149.43	0.27
	B41	120	2.0	1.47	126.54	112.72	10.92
	B42	120	2.0	1.96	143.76	129.78	9.72
	B43	120	2.5	1.47	103.63	101.04	2.49
	B43	120	2.5	1.47	103.63	101.04	2.49
	B44	120	2.5	1.96	126.54	116.34	8.06
	B45	120	3.0	1.47	80.68	92.41	-14.53
	B46	120	3.0	1.96	94.19	106.40	-12.96
	B47	120	3.5	1.47	66.95	85.69	-27.99
	B48	120	3.5	1.96	77.87	98.66	-26.69
	NBH1	0	2.1	1.96	190	189.34	0.34
	BH1	60	2.1	1.96	170	152.78	10.13
	BH2	90	2.1	1.96	142	134.38	5.36
	BH3	90	2.1	1.96	115	132.30	-15.04
	BH4	120	2.1	1.96	120	126.72	-5.59
	NBH2	0	2.6	1.96	175	158.58	9.38
	BH5	90	2.6	1.96	140	119.99	14.28
Table 2	BH6	90	2.6	1.96	98.5	118.77	-20.58
	NBH3	0	3.3	1.96	140	130.11	7.06
	BH7	90	3.3	1.96	110	105.76	3.86
	NBH4	0	2.1	1.96	180	130.11	27.71
	BH8	90	2.1	1.61	138	128.19	7.10
	NBH5	0	2.1	1.96	170	142.28	16.30
	BH9	90	2.1	1.47	125	122.15	2.27

6. Conclusions

In this paper, shear strength tests of five room-temperature beams and nine post-fire beams without stirrups were conducted, and the factors that influenced the shear capacity were investigated. Based on ABAQUS, a numerical analysis method of RC beams after fire exposure was established, and a simplified calculation formula was proposed to evaluate the shear capacity of post-fire beams without stirrups. The following conclusions can be drawn:

1. The shear capacity and stiffness of the specimens decreased after fire exposure, and the shear strength loss of the beams increased with fire time. Compared with the beam at ambient temperature, the residual shear capacity of beams subjected to fire on three sides for 60 min, 90 min and 120 min were reduced by 10.5%, 24.7% and 36.8%, respectively.
2. The shear capacity and the stiffness of fire-damaged specimens decreased as the shear span ratio λ increased, and the shear strength loss of the beams decreased with λ . For the beams without stirrups subjected to fire on three sides for 90 min, the residual shear capacity of beams with different shear span ratios of 2.1, 2.6 and 3.3 were reduced by 24.7%, 20.0% and 17.8%, respectively.
3. The shear capacity of fire-damaged specimens increased as the longitudinal reinforcement ratio ρ increased, and the shear strength loss of the beams increased with the longitudinal reinforcement ratio ρ . For the beams without stirrups subjected to fire on three sides for 90 min, the residual shear capacity of beams with different longitudinal reinforcement ratios of 1.47%, 1.61% and 1.96% were reduced by 8.8%, 12.2% and 24.7%, respectively.
4. Comparing the theoretical results and the experimental results, the theoretical value of the beam without stirrups after fire exposure is in good agreement with the experimental valued, and the average absolute error is 10.48%, so this formula can still evaluate the shear capacity of post-fire beams without stirrups with acceptable accuracy.
5. The findings of this study are expected to be useful to researchers and designers looking to improve the performance of beams without stirrups when exposed to fire. However, the theoretical study on shear capacity of RC beams after fire exposure were not conducted in this study, and should be further investigated in future researches.

Author Contributions: Conceptualization, Y.S. and C.F.; Methodology, Y.S. and S.L.; software, Y.S.; investigation, Y.S. and C.F.; resources, C.F. and S.L.; writing—original draft preparation, Y.S.; writing—review and editing, Y.S.; All authors have read and agreed to the published version of the manuscript.

Funding: Funded by National natural Science Foundation of China (No. 51478254).

Informed Consent Statement: Informed consent was obtained from all subjects involved in the study.

Data Availability Statement: Not applicable.

Acknowledgments: The authors disclosed receipt of the following financial support for the research, authorship, and/or publication of this article.

Conflicts of Interest: The authors declare no conflict of interest.

References

1. Xiao, J.Z.; Li, J.; Sun, Z.P. Review of studies on the fire-resistance behaviour of HPC structures. *Ind. Constr.* **2001**, *31*, 53–56.
2. Zhang, Z.M.; Ye, Z.M.; Liu, T. Research progress in fire resistance of reinforced concrete structures. *J. Nat. Disasters* **2007**, *16*, 127–135.
3. Jiang, C.J.; Yu, J.T.; Li, L.Z.; Wang, X.; Wang, L.; Liao, J.H. Experimental study on the residual shear capacity of fire-damaged reinforced concrete frame beams and cantilevers. *Fire Saf. J.* **2018**, *100*, 140–156. [[CrossRef](#)]
4. Xing, Q.; Liao, J.H.; Chen, Z.; Huang, W. Shear behaviour of fire-damaged reinforced-concrete beams. *Mag. Concr. Res.* **2020**, *72*, 357–364. [[CrossRef](#)]
5. Higuchi, K.; Keitai, I.; Koichi, M. Remaining shear capacity of fire-damaged high strength RC beams after moist curing. *J. Adv. Concr. Technol.* **2021**, *19*, 897–912. [[CrossRef](#)]

6. Fu, C.G.; Wang, G.Y.; Wang, Y.Z. The Temperature field analysis of reinforced concrete frame joints under fire. *J. Shandong Jianzhu Univ.* **2009**, *24*, 1–8+17.
7. Fu, C.G.; Song, Y.M.; Yin, A.K.; Liang, S.T.; Yam, K. Experimental study on shear bearing capacity of reinforced concrete beams under thermodynamic coupling. *J. Shandong Jianzhu Univ.* **2018**, *33*, 1–10+23.
8. Liu, F.T.; Wo, B.; Wei, D.M. Failure Models of Reinforced Concrete Beams Strengthened with Carbon Fiber Sheet in Fire. *Fire Saf. J.* **2009**, *44*, 941–950. [[CrossRef](#)]
9. Ng, A.H.B.; Mirza, M.S.; Lie, T.T. Response of Direct Models of Reinforced Concrete Columns Subjected to Fire. *ACI Struct. J.* **1990**, *87*, 313–323.
10. Lie, T.T.; Irwin, R.J. Method to Calculate the Fire Resistance of Reinforced Concrete Columns with Rectangular Cross Section. *ACI Struct. J.* **1993**, *90*, 52–60.
11. El-Hawary, M.M.; Ragab, A.M.; El-Azim, A.A.; Elibiari, S. Effect of fire on flexural behaviour of RC beams. *Constr. Build. Mater.* **1996**, *10*, 147–150. [[CrossRef](#)]
12. El-Hawary, M.M.; Ragab, A.M.; El-Azim, A.A.; Elibiari, S. Effect of fire on shear behaviour of RC beams. *Constr. Build. Mater.* **1997**, *65*, 281–287.
13. ISO 834; Fire-Resistance Tests: Elements of Building Construction, Part 1.1: General Requirements for Fire Resistance Testing. ISO—International Organization for Standardization: Geneva, Switzerland, 1999.
14. Hibbitte, K. *ABAQUS User Subroutines Reference Manual*; 1–3 Version 6.5; Hibbitt, Karlsson and Sorensen, Inc.: Pawtucket, RI, USA, 2006.
15. *GB 50010-2010*; Code for Design of Concrete Structures. China Architecture and Building Press: Beijing, China, 2015.
16. Elloboby, E.; Bailey, C.G. Modelling of unbounded post-tensioned concrete slabs under fire conditions. *Fire Saf. J.* **2009**, *44*, 159–169. [[CrossRef](#)]
17. *EN 1991-1-2*; Eurocode 1: Actions on Structures, Part 1–2: General Actions-Actions on Structures Exposed to Fire. European Committee for Standardization: Brussels, Belgium, 2002.
18. Lie, T.T.; Denham, E.M.A. *Factors Affecting the Fire Resistance of Circular Hollow Steel Columns Filled with Bar-Reinforced Concrete*; NRC-CNRC Internal Report; National Research Council of Canada: Ottawa, ON, Canada, 1993.
19. Guo, Z.H.; Shi, X.D. *Experimental and Calculation of Reinforced Concrete at Elevated Temperatures*; Tsinghua University Press: Beijing, China, 2011.
20. Kook-Han, K.; Sang-Eun, J.; Jin-Keun, K.; Sungchul, Y. An experimental study on thermal conductivity of concrete. *Cem. Concr. Res.* **2003**, *33*, 363–371.
21. Lu, Z.D. *Research on the Response of Reinforced Concrete Beams to Fire*; Tongji University: Shanghai, China, 1989; pp. 23–31.
22. Lie, T.T.; Lin, T.D.; Allen, D.E.; Abrams, M.S. *Fire Resistance of Reinforced Concrete Columns*; Division of Building Research, DBR Report, No. 1167; National Research Council of Canada: Ottawa, ON, Canada, 1984.
23. Guo, Z.H.; Li, W. *The Summary of Experimental Research on Thermal Mechanical Properties of Concrete*; Department of Civil Engineering, Tsinghua University: Beijing, China, 1991.
24. *ENV 1993-1-2*; Eurocode 3, Design of Steel Structures, Part 1.2: General Rules-Structural Fire Design. European Committee for Standardization: Brussels, Belgium, 2005.
25. Elmoussa, B.; Temsah, Y.; Jahami, A. Numerical study for the effect of hairpin shaped shear reinforcement on one-way shear capacity of reinforced concrete beams. *MATEC Web Conf.* **2019**, *281*, 01015. [[CrossRef](#)]
26. Zsutty, T.C. Beam shear strength prediction by analysis of existing data. *ACI J. Proc.* **1968**, *65*, 943–951.
27. Liao, J.H.; Lu, Z.D.; Su, L. Experiment and finite element analysis of shear strength of concrete beams subjected to elevated temperature. *J. Tongji Univ. Nat. Sci.* **2013**, *41*, 806–812.
28. Liao, J.H.; Lu, Z.D.; Yu, J.T. Effect of loads during high temperature on shear strength of reinforced concrete beams after fire. *J. Build. Struct.* **2013**, *34*, 30–36.